Thin coatings thickness measurement by augmented nanoindentation data fusion

CIRP Annals - Manufacturing Technology 73 (2024) 409–412

Contents lists available at ScienceDirect

CIRP Annals - Manufacturing Technology

journal homepage: https://www.editorialmanager.com/CIRP/default.aspx

Thin coatings thickness measurement by augmented nanoindentation data fusion

Gianfranco Genta*, Giacomo Maculotti

Department of Management and Production Engineering, Politecnico di Torino, Corso Duca degli Abruzzi 24, 10129 Torino, Italy

Submitted by Raffaello Levi (1), Politecnico di Torino, Italy

ARTICLE INFO

Article history:
Available online 21 May 2024

Keyword:
Nano indentation
Coating
Machine learning

ABSTRACT

Layer thickness of thin and multi-layer coatings is a major design parameter to functionalise surfaces in a broad range of industrial applications. Conventional measurement methods are often complex, expensive, and limited in thickness range and applicability, particularly for thin coatings on fragile substrates and/or with complex compositions. An innovative methodology is introduced based on nanoindentation, leveraging data fusion and nanoindentation augmentation with in-situ current measurement, to evaluate functional and physical layer thickness by material properties and statistical modelling techniques. Two cases concerning coatings for semiconductor and tribomechanical applications are described, exhibiting faster, cheaper, and metrologically competitive results over current techniques.

1. Introduction

Advanced high-performance surface coating technologies are a strategic engineering tool for tailoring surface properties [1]. Their substantial worldwide market value is shared primarily among Asia (45 %), EU and USA (42 %), due to their predominant lead in the semiconductor industry [2].

These coatings are applied in the semiconductor industry to improve the energy efficiency and durability of energy harvesting devices by increasing surface passivation [3]. Mechanical applications often rely on composite and multi-layer coatings to improve tribological and wear-resistance properties, thus extending the service life of components [4]. Specific applications can be found in manufacturing, where the adoption of coated cutting tools has shown increased machining quality [4,5], and in optics manufacturing accuracy thanks to coated moulds [5]. The automotive sector widely uses coatings to enhance the mechanical durability of core engine parts while reducing fuel consumption and pollutant emissions [6]. Similarly, ultra-thin multi-layered coatings allow functionally improved performances of materials in aggressive environments due to high corrosion and extreme temperatures, thus being highly attractive, e.g., in aerospace [7].

Coating layers thickness is often a functional parameter to be controlled, for it can impact on tribo-mechanical properties, microstructural integrity, strength, and fatigue [8–10]. Furthermore, to allow mechanical characterisation of the coated system, often by nanoindentation [11], the layers' thickness must be known [12,13]. Therefore, both during process optimization and quality control, measurement of coating thickness is essential. However, this often represents a challenge for multi-layer and thin coatings. Several approaches are available in the literature. Some are destructive techniques, e.g. ball cratering test and cross-sectioning followed by optical microscope inspection [8]. However, the former might be easily and robustly applicable only to thicker coatings (thickness larger than 1 µm), while the latter presents severe limitations for fragile substrate, e.g. semiconductors and ceramics, and for highly plastic coatings, e.g. PTFE-based coatings [14]. Also, cross-sectioning traceability is hard to establish due to challenges in calibration and uncertainty evaluation of the measurement. Alternatives are based on non-destructive techniques such as white light interferometry (WLI), X-ray diffraction (XRD), µ-X-ray computed tomography (µ-XCT), and laser-based approaches. WLI is limited to transparent films, and uncertainties do not allow measurements of thin and ultra-thin layers [15]. XRD can be highly flexible and copes with several thickness ranges, but it is quite an expensive technique [16,17] and not highly practical for industrial applications of routine quality control. Similar limitations are shared by µ-XCT, whose accuracy is affected by high material heterogeneity due to possible largely different densities [18]. Other unconventional methods have been proposed leveraging the photothermal effect and have been applied for thickness down to the micrometre, but they require a complex experimental setup [19].

A method based on nanoindentation is proposed to measure the thickness of multi-layered coating systems through a quick and cost-effective empirical procedure, allowing high precision of results when data augmentation and sensor-fusion are exploited, offering an attractive alternative to conventional approaches. Furthermore, nanoindentation allows establishing traceability and evaluating measurement uncertainty of the estimated thickness conveniently and more easily than other approaches. Section 2 presents the modelling of the material behaviour and the statistical approach proposed to measure the thickness. Section 3 deals with the application of the proposed method to industrially relevant case studies in a wide range of thicknesses, and comparison with alternative methods currently used in industry and academia. Finally, Section 4 draws conclusions.

2. Methodology

2.1. Material mechanical behaviour modelling

Fig. 1(a) shows schematic modelling of a multi-layer coating system, consisting of n layers and a substrate. The thickness of each layer t_i ($i = 1, \ldots, n, n+1$, the substrate being the n + 1-th layer) depends on deposition process parameters, and its dispersion is significantly affected, for thin layers, by the surface topography of the underlying layers. In simpler cases, layers can be distinguished by discontinuity in the material structure and

* Corresponding author.
E-mail address: gianfranco.genta@polito.it (G. Genta).

https://doi.org/10.1016/j.cirp.2024.04.093

associated with physical interfaces. However, transition interfaces may be present depending on the deposition process and the chemical affinity between the coating and the coated material, as shown in Fig. 1(b). Accordingly, for the i th layer, two characteristic thicknesses may be identified. The first, related to the functional interface t_{fi}, is the maximum depth before the onset of the transition and represents the volume of material mechanically unaffected by the following layers, assuming that $(t_{fi} - t_{i-1}) < (t_i - t_{i-1})/10$ [12,13]. The second is the physical interface, t_i, i.e. the depth beyond which the effect of the subsequent $i + 1$ layer is predominant. The knowledge of such characteristic thicknesses is relevant to designing materials and manufacturing for functionally graded applications.

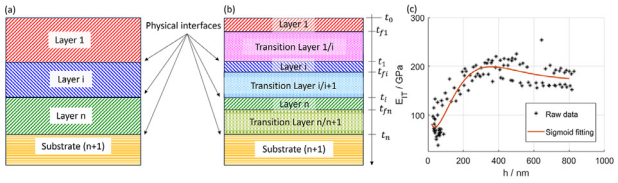

Fig. 1. (a) Schematic representation of a multi-layer coating system with (b) indication of transition layers. (c) Typical mechanical response E_{IT} from nanoindentation of a 550 nm SiO_2/Si<100>.

Nanoindentation is conventionally used to evaluate the mechanical response of coated systems in terms of indentation modulus E_{IT} and indentation hardness H_{IT} [8,11,12], while distinguishing between the layers' and substrate effect [13,20]. Nanoindentations can be conveniently performed in continuous multi-cycle (CMC), i.e. by applying a series of quasistatic indentations in the same position with increasing maximum force. By analysing several unloading curves at increasingly maximum penetration depths h, the material response may be characterised as a function of h, without cross-sectioning the sample [12,13]. Fig. 1(c) shows a typical mechanical response in terms of the indentation modulus of a single-layer coating, where a transition to a constant value of the substrate is visible. The transient is induced by such effects as material structure, deposition process phenomena, and by the mechanical stress state tensor of the material due to nanoindentation. In fact, beyond a certain penetration depth, even for $h < t_i$, the stress tensor begins to involve the underneath layer, thus introducing a convolution in the mechanical response of the material [13,20,21]. The resulting behaviour can be modelled as a log-logistic sigmoid [22]:

$$M = g(h;\boldsymbol{\vartheta}) = \vartheta_1 + \frac{\vartheta_2 - \vartheta_1}{e^{\frac{h-\vartheta_3}{\vartheta_4}}} \tag{1}$$

where M is any material response evaluated by CMC nanoindentation, the parameters $\boldsymbol{\vartheta}$ are to be fitted by nonlinear regression, see e.g. Fig. 1(c).

2.2. Thickness evaluation by nanoindentation data-fusion

The convolution of the mechanical response probability distribution can be modelled as a Gaussian mixture model (GMM) [21]. A higher resolution model is proposed here, considering the transition layers, as in Fig. 1(b), in addition to layers and the substrate:

$$\begin{aligned} M \sim GMM(\boldsymbol{\theta}) &= GMM(\boldsymbol{\mu}, \Sigma; \boldsymbol{\pi}) = \sum_{k=1}^{2n+1} \pi_k N(\mu_k, \sigma_k^2) \\ &= \sum_{i=1}^{n+1} \pi_i N(\mu_i, \sigma_i^2) + \sum_{j=1}^{n} \pi_{j/j+1} N\left(\mu_{j/j+1}, \sigma_{j/j+1}^2\right) \end{aligned} \tag{2.1}$$

$$f_M = f_M(m|\boldsymbol{\theta}) = \sum_{k=1}^{2n+1} \pi_k f_{M,k}(m|\{\mu_k, \sigma_k^2\}) \tag{2.2}$$

where μ_i and σ_i^2 are the average and variance of the mechanical response of the layer within the functional depth, thus unaffected by other layers, i.e. for $t_{i-1} < h < t_{fi}$. Transition layers, i.e. for $t_{fi} < h < t_i$ as in Fig. 1(a), are related to $\mu_{j/j+1}, \sigma_{j/j+1}^2$. The GMM is a weighted sum of the contributions with weights π_i and $\pi_{j/j+1}$ and related constraints, i.e. $\pi_i, \pi_{j/j+1} \in]0;1[\; \forall \; i, j$ and $\sum_{i=1}^{n+1} \pi_i + \sum_{j=1}^{n} \pi_{j/j+1} = 1$. From empirical data, deconvolution procedures based on expectation maximization estimate the parameters of the posterior probability of the k-th mixture component, thus evaluating $f_{M,k}$, i.e. probability density functions (pdf) [21,23], as per Eq. (2.2).

GMM may be exploited to classify realisation m of the stochastic variable M to the mixture components' contributions [23]. This can be performed by evaluating the maximum a-posteriori probability (MAP) that the realization is due to the k-th component, as in Eq. (3.1), and the most probable class may be identified according to the hard clustering criterion, as in Eq. (3.2).

$$p(z_i = k|m, \boldsymbol{\theta}) = \frac{\pi_k f_{M,k}(m)}{f_M(m|\boldsymbol{\theta})} \tag{3.1}$$

$$\begin{aligned} z_i &= \underset{k}{\operatorname{argmax}}\{p(z_i = k|m, \boldsymbol{\theta})\} \\ &= \arg\max_k\{\log(f_{M,k}(m)) + \log(\pi_k)\} \end{aligned} \tag{3.2}$$

Accordingly, introducing a mis-classification risk of error of type I, related to the k-th coating layer, i.e. α_k, a threshold value of the mechanical response M_k^* may be identified to ensure a classification probability with a confidence level $P_k = 1 - \alpha_k$. In particular, assuming an increasing trend for $M = g(h;\boldsymbol{\vartheta})$, and considering the definitions of t_{fi} and t_i, it is possible to evaluate:

$$M_{fi}^* = \min\{M : p(k = 2i - 1|M, \boldsymbol{\theta}) = 1 - \alpha_{2i-1}\} \tag{4.1}$$

$$M_i^* = \max\{M : p(k = i + 2|M, \boldsymbol{\theta}) = \alpha_{i+2}\} \tag{4.2}$$

Similar equations might be written for decreasing $M = g(h;\boldsymbol{\vartheta})$. The evaluation of the threshold value M_{fi}^* and M_i^* allows estimating, at a given risk of error of type I, the associated penetration depth $h_{M,k}^* = g^{-1}(M_k^*)$ obtained by inverting the model estimated in Eq.(1). In particular, $t_{fi} = g^{-1}(M_{fi}^*)$ and $t_i = g^{-1}(M_i^*)$ will hold. Furthermore, the standard uncertainty of the evaluated characteristic depth $u(h_{M,k}^*)$ may be obtained by propagating the measurement reproducibility of M, h and the model parameters ϑ regression estimation uncertainty, according to the law of uncertainty propagation [24]:

$$u^2\left(h_{M,k}^*\right) = \sum_{w=1}^{4} \left.\frac{\partial g^{-1}(M;\boldsymbol{\vartheta})}{\partial \vartheta_w}\right|_{\vartheta_w^*}^2 \cdot u^2(\vartheta_w) + \left.\frac{\partial g^{-1}(M;\boldsymbol{\vartheta})}{\partial M}\right|_{M_k^*}^2 \cdot u^2(M) + u^2(h) \tag{5}$$

Different nanoindentation mechanical responses exhibit diverse sensitivity to material transition. Furthermore, nanoindentation data may be augmented through in-situ measurement of electric current by electric contact resistance (ECR) [25]. ECR provides insights into the phase and structure of the probed material by measuring the resistance R between a conductive indenter and the material. The resistance would exhibit changes of orders of magnitude when passing from one layer to another with different resistivity. Thus, material responses, let $\boldsymbol{M} = \{E_{IT}, H_{IT}, R\}$, can be combined leveraging on competitive data fusion to improve the accuracy and the precision of the estimation of the characteristic depths $h_{M,k}^*$ [26,27]. In this work, inverse-variance weighting (IVW) is applied to achieve data fusion (DF), considering the three material responses $\boldsymbol{M}$ evaluated by nanoindentation, as per Eq.(6). In the case of marginal normal probability distributions, IVW guarantees the correctness of the mean estimation, since Eq.(6.1) is the maximum likelihood estimate of the true value, while minimizing the variance of the combination [23].

$$\widehat{h_{DF,k}^*} = \frac{\sum_{m=1}^{3} h_{m,k}^*/u^2(h_{m,k}^*)}{\sum_{m=1}^{3} 1/u^2(h_{m,k}^*)} \tag{6.1}$$

$$u^2\left(\widehat{h_{DF,k}^*}\right) = \frac{1}{\sum_{m=1}^{3} 1/u^2(h_{m,k}^*)} \tag{6.2}$$

3. Case studies

3.1. Materials and methods

The proposed methodology based on nanoindentation data fusion to evaluate the thickness of coating systems is applied to two case studies: i) a monolayer system SiO_2/Si<100> obtained by atmospheric pressure chemical vapour deposition with a nominal thickness of 550 nm, typical to improve surface passivation in semiconductor industry [3] and, ii) a multi-layer coating PTFE+Pb/Bronze/SS obtained by casting PTFE reinforced with fine particles of Pb on porous sintered Bronze over a stainless steel (SS) backing, with an overall coating thickness of 300 µm, used in bushings as a solid lubricant for linear pneumatic actuators [14,28]. Pb particle dispersion was found to leave a uniform outermost layer [28].

Instrumented indentation tests were performed by state-of-the-art platform Anton Paar STePP6 in a metrological room [25]. Specifically, the SiO_2/Si<100> was characterised with the NHT^3 head performing 30 CMC nanoindentations with 45 cycles from 0.5 mN to 100 mN with a loading-holding-unloading duration of 60 s each. Conversely, the PTFE+Pb/Bronze/SS was investigated with the MCT^3 head performing 40 CMC indentations with 30 cycles from 0.5 N to 30 N, with a loading-holding-unloading duration of 30 s each [12,13]. Only the tribological coating was additionally investigated with ECR due to the high resistivity of SiO_2. Experimental setup and specimens are shown in Fig. 2.

Surface topography was also measured to complement the analysis using a CSI Zygo NewView9000 with a 20 × magnification objective for the SiO_2 and a 5 × for the PTFE+Pb; measurement setup details, bandwidth specification [29] for the characterisation of the SL-surface, and results are reported in Table 1.

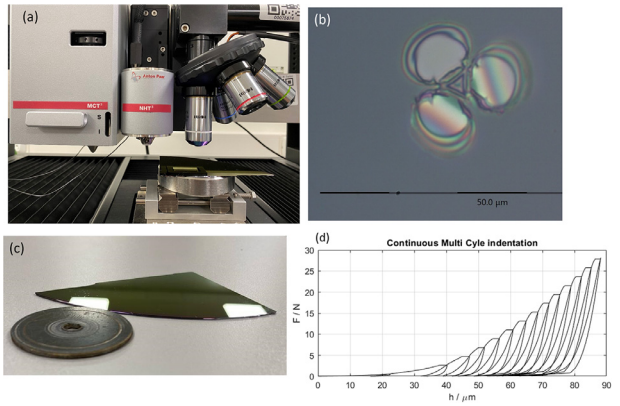

Fig. 2. (a) STeP6 Anton Paar indentation platform for ECR and section of SiO_2/Si<100> wafer; (b) nanoindentation on SiO_2; (c) measured specimens: SiO_2/Si<100> wafer fragment and a PTFE+Pb/Bronze/SS disc; (d) a PTFE+Pb/Bronze/SS CMC indentation curve (force vs penetration depth).

Table 1
Surface topography measurement setup details (field of view - FoV) and results. Uncertainty was evaluated considering as dominating contribution the reproducibility [30] with a coverage factor of 2.

Sample	FoV	Bandwidth	*Sa* / nm	*Sq* / nm
SiO_2	(0.43 × 0.43) mm (1000 × 1000) pxl	N_{is} = 2 µm, N_{ic} = 0.2 mm	0.23 ± 0.01	0.29 ± 0.11
PTFE+Pb	(1.53 × 1.53) mm (1000 × 1000) pxl	N_{is} = 5 µm, N_{ic} = 0.5 mm	950 ± 220	1470 ± 320

Other thickness measurement methods currently employed in industry and academia were considered to compare performances with the proposed approach.

In particular, XRD has been used for the SiO_2/Si<100>. Measurement uncertainty will be reported propagating the literature reference value of 3 % as a type B contribution [31].

PTFE+Pb/Bronze/SS sample's larger size allowed more alternatives. Cross-section inspection was performed under a metallographic optical microscope (OM) Leica Z16. To evaluate reproducibility, 5 images in the cross-section and measures of 25 locations each were performed, see Fig. 3(a); uncertainty was reported propagating the contribution of the calibration of 50 nm and the reproducibility. Last, µ-XCT was performed with a custom built Fraunhofer Institute XCT [32], measuring a thin slice of the sample with 800 projections, see Fig. 3(b), with a tube current of 120 µA, an acceleration voltage of 260 kV, with a Surgent-Objective-Distance of 50 mm and a Surgent-Detector-Distance of 1200 mm, resulting in a voxel size of 8 µm. Separation of the grey-scale intensity was relied upon to distinguish the edges of the layers through a machine vision algorithm.

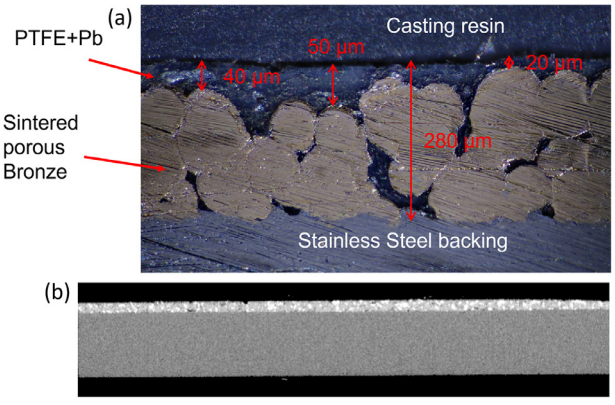

Fig. 3. Thickness measurement of PTFE+Pb/Bronze/SS with (a) OM cross-section with marked measured dimensions of the layers, (b) µ-XCT.

3.2. Results and discussion

Fig. 4 shows the material responses of the two considered samples. Raw data (black asterisks) show the sigmoid trend of Eq. (1), which resulted in the red trend after nonlinear regression.

The SiO_2/Si<100>, due to the relative negligible change in H_{IT}, allowed applying the method only to the E_{IT}. GMM deconvolution evaluated

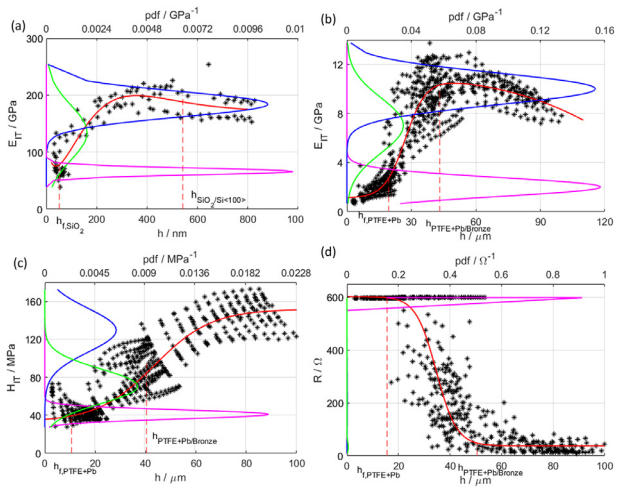

Fig. 4. Material response (M) against penetration depth h. Black asterisks: raw data; continuous red line: fitting; magenta: pdf of outermost layer; green: pdf of transition layer; blue: pdf of innermost measured layer; red dashed lines: measured thicknesses. (a) E_{IT} of SiO_2/Si<100>. PTFE+Pb/Bronze/SS: (b) E_{IT}, (c) H_{IT} (the systematic trend in raw data subgroups is due to the definition of H_{IT} as a function of $1/h^2$), (d) R (the pdf of the Transition layer in green and the Bronze layer in blue are hardly visible due to the large predominance of the insulating layer, i.e. PTFE+Pb).

components' probability distributions and, with a risk of error of 5 %, resulted in the characteristic depths marked in the figures. In particular, the functional depth h_{f,SiO_2} of the SiO_2 layer evaluation was (52±15) nm, compatible with the literature indication of 10 % of the coating depth [12,13]. The physical interface $h_{SiO_2/Si\langle 100\rangle}$ resulted of (542±84) nm, compatible with XRD evaluation of (566±17) nm.

The PTFE+Pb/Bronze/SS coating material enables the application of data fusion and data augmentation. First, the greater dispersion of the raw data in Fig. 4(b–d) may be associated to the larger roughness and porous nature of the second layer. Second, data augmentation yielding the resistance measurement identifies a first dielectric layer, i.e. the PTFE+Pb with high constant R, followed by a transition with large dispersion; the additional presence of insulating material at larger depths is consistent with PTFE+Pb material pockets created by the pouring process into the porous bronze matrix, see Fig. 3(a). This induces heteroscedasticity in thickness evaluations based on R, see Fig. 5.

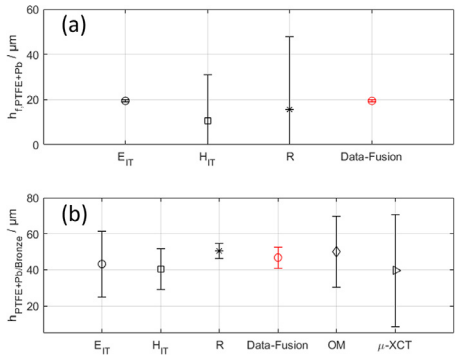

Fig. 5. (a) Functional thickness and (b) interface thickness of PTFE+Pb. Error bars represent uncertainty at 95 % confidence level. In (a) ordinates are truncated to exclude non-physical values.

The maximum force range allowed penetration down to 100 µm; thus, only the functional and the interface thickness of the PTFE+Pb layer could be investigated by the proposed technique, which provided results shown in Fig. 5. The results show higher metrological performances, in terms both of accuracy and precision, of the proposed approach with respect to other alternatives, thanks to data fusion. While results are compatible, the resolution strongly limits both OM and µ-XCT.

Furthermore, as shown in both case studies, the proposed approach is more informative, since other techniques are unable to evaluate functional layer thickness. The proposed approach resulted in an estimation with a relative uncertainty of 2.5 % for $h_{f,PTFE+Pb}$ and of 10 % for $h_{PTFE+Pb/Bronze}$, against over 40 % exhibited by OM and µ-XCT for the latter case.

4. Conclusions

A methodology based on material behaviour and statistical modelling is proposed to evaluate multi-layer coating thickness. The approach, demonstrated in two case studies, leverages in-situ electrical measurement augmentation instrumented indentation test and data fusion. The method is more informative and accurate than others currently resorted to in industry and academia; being also less complex and resource intensive, it provides a practical tool to inspect coating thickness, an essential design parameter for surface functionalisation.

Declaration of competing interest

The authors declare that they have no known competing financial interests or personal relationships that could have appeared to influence the work reported in this paper.

CRediT authorship contribution statement

Gianfranco Genta: Conceptualization, Formal analysis, Funding acquisition, Methodology, Project administration, Resources, Supervision, Validation, Writing – review & editing. **Giacomo Maculotti:** Conceptualization, Data curation, Formal analysis, Investigation, Methodology, Software, Validation, Visualization, Writing – original draft.

Acknowledgments

The authors thank Prof. Maurizio Galetto for the fruitful discussions. Work funded by 22RTP01 TracInd BVK-H EPM and EU Horizon Europe Research and Innovation Programme.

References

[1] Bruzzone AAG, Costa HL, Lonardo PM, Lucca DA (2008) Advances in Engineered Surfaces for Functional Performance. *CIRP Annals* 57:750–769.
[2] www.statista.com. Last visited 22/12/2023
[3] Yan D, Cuevas A, Stuckelberger J, Wang EC, Phang SP, Kho TC, et al. (2023) Silicon Solar Cells with Passivating Contacts: Classification and Performance. *Progress in Photovoltaics Research and Applications* 31:310–326.
[4] Bemporad E, Sebastiani M, Pecchio C, De Rossi S (2006) High Thickness Ti/TiN Multilayer Thin Coatings for Wear Resistant Applications. *Surface & Coatings Technology* 201:2155–2165.
[5] Mehner A, Zoch HW, Datchary W (2006) Pongs G Sol-gel Coatings for High Precision Optical Molds. *CIRP Annals* 55:589–592.
[6] Bewilogua K, Bräuer G, Dietz A, Gäbler J, Goch G, Karpuschewski B, et al. (2009) Surface Technology for Automotive Engineering. *CIRP Annals* 58:608–627.
[7] Anirudh S, Krishnamurthy S, Kandasubramanian B, Kumar B (2023) Probing into Atomically Thin Layered Nano-materials Protective Coating for Aerospace and Strategic Defence Application – A Review. *The Journal of Alloys and Compounds* 968:172203.
[8] Bouzakis KD, Michailidis N, Skordaris G, Bouzakis E, Biermann D, M'Saoubi R (2012) Cutting with Coated Tools: Coating Technologies, Characterization Methods and Performance Optimization. *CIRP Annals* 61:703–723.
[9] Bouzakis K-D, Hadjiyiannis S, Skordaris G, Anastopoulos J, Mirisidis I, Michailidis N, et al. (2003) The Influence of the Coating Thickness on its Strength Properties and on the Milling Performance of PVD Coated Inserts. *Surface and Coatings Technology* 174–175:393–401.
[10] Gu P, Zhu C, Mura A, Maculotti G, Goti E (2022) Grinding Performance and Theoretical Analysis for a high volume Fraction SiCp/Al Composite. *Journal of Manufacturing Processes* 76:796–811.
[11] Lucca DA, Klopfstein MJ, Ghisleni R, Gude A, Mehner A (2004) Datchary W Investigation of Sol-gel Derived ZrO_2 Thin Films by Nanoindentation. *CIRP Annals* 53:475–478.
[12] Bull SJ (2005) Nanoindentation of Coatings. *Journal of Physics D: Applied Physics* 38:R393–R413.
[13] Puchi-Cabrera ES, Staia MH, Iost A (2015) Modeling the Composite Hardness of Multilayer Coated Systems. *Thin Solid Films* 578:53–62.
[14] Goti E, Mazza L, Manuello Bertetto A (2020) Wear Tests on PTFE+pb Linings for Linear Pneumatic Actuator Guide Bushings. *The International Journal and Mechanics and Control* 21:155–162.
[15] Dong JT, Lu RS (2012) Sensitivity Analysis of Thin-film Thickness Measurement by Vertical Scanning White-light Interferometry. *Applied Optics* 51:5668–5675.
[16] Brinksmeier E, Lucca DA, Walter A (2004) Chemical Aspects of Machining Processes. *CIRP Annals* 53:685–699.
[17] Lucca DA, Brinksmeier E, Goch G (1998) Progress in Assessing Surface and Subsurface Integrity. *CIRP Annals* 47:669–693.
[18] Dewulf W, Bosse H, Carmignato S, Leach R (2022) Advances in the Metrological Traceability and Performance of X-ray Computed Tomography. *CIRP Annals* 71:693–716.
[19] Goch G, Prekel H, Patzelt S, Ströbel G, Lucca DA, Stock HR, et al. (2004) Non-destructive and Non-contact Determination of Layer Thickness and Thermal Properties of PVD and Sol-gel Layers by Photothermal Methods. *CIRP Annals* 53:471–474.
[20] Chen S, Liu L, Wang T (2005) Investigation of the Mechanical Properties of Thin Films by Nanoindentation, Considering the Effects of Thickness and Different Coating-substrate Combinations. *Surface & Coatings Technology* 191: 25–32.
[21] Huen WY, Lee H, Vimonsatit V, Mendis P, Lee HS (2019) Nanomechanical Properties of Thermal arc Sprayed Coating using Continuous Stiffness Measurement and Artificial Neural Network. *Surface & Coatings Technology* 366: 266–276.
[22] Lorenz L, Chudoba T, Makowski S, Zawischa M, Schaller F (2021) Weihnacht V Indentation Modulus Extrapolation and Thickness Estimation of ta-C Coatings from Nanoindentation. *The Journal of Materials Science* 56:18740–18748.
[23] Murphy KP (2012) *Machine Learning: A Probabilistic PerspectiveCambridge*, The MIT PressMA.
[24] Anon (2008) *JCGM100: Evaluation of Measurement Data — Guide to the Expression of Uncertainty in Measurement (GUM)*, SèvresFrance.
[25] Galetto M, Kholkhujaev J, Maculotti G (2023) Improvement of Instrumented Indentation Test Accuracy by Data Augmentation with Electrical Contact Resistance. *CIRP Annals* 72:469–472.
[26] Franceschini F, Galetto M, Maisano D, Mastrogiacomo L (2016) Combining multiple Large Volume Metrology Systems: Competitive versus Cooperative Data Fusion. *Precision Engineering* 43:514–524.
[27] Schmitt RH, Peterek M, Morse E, Knapp W, Galetto M, Härtig F, et al. (2016) Advances in Large-Scale Metrology – Review and Future Trends. *CIRP Annals* 65:643–665.
[28] Maculotti G, Goti E, Genta G, Mazza L, Galetto M (2024) Comprehensive Mechanical and Tribological Characterization of Metal-polymer PTFE+Pb/Bronze Coating by in-situ Electrical Contact Resistance Measurement Augmented Tribo-mechanical Tests. *Tribology International* 193:109397.
[29] Anon (2024) ISO 25178-2:2021. *Geometrical Product Specifications (GPS) — Surface Texture. Areal Part 2*: Terms, Definitions and Surface Texture Parameters, ISO-Genève.
[30] Tosello G, Haitjema H, Leach RK, Quagliotti D, Gasparin S, Hansen HN (2016) An International Comparison of Surface Texture Parameters Quantification on Polymer Artefacts using Optical Instruments. *CIRP Annals* 65:529–532.
[31] Aliaj FR, Syla N, Oettel H, Dilo T (2017) Thickness Determination of TiN and TiAl Coatings on Steel Substrates using X-ray Diffraction method and their Composition Measurements by GD-OES. *Surface and Interface Analysis* 49:1135–1141.
[32] www.j-tech.polito.it/facilities/technical_data/ct_scan. Last visited 15/03/2024.